

# On the Robustness of Cluster Clustering Covariance Calibration

A. Fumagalli<sup>1</sup> \*, T. Castro<sup>2,3,4,5</sup> \*\*, S. Borgani<sup>6</sup>, 2, 3, 4, 5 and M. Valentini<sup>6</sup>, 2, 3, 4, 5

<sup>1</sup> Ludwig-Maximilians-University, Schellingstrasse 4, 80799 Munich, Germany

<sup>2</sup> INAF - Osservatorio Astronomico di Trieste, Via G. B. Tiepolo 11, 34143 Trieste, Italy

<sup>3</sup> IFPU, Institute for Fundamental Physics of the Universe, via Beirut 2, 34151 Trieste, Italy

<sup>4</sup> INFN, Sezione di Trieste, Via Valerio 2, 34127 Trieste TS, Italy

<sup>5</sup> ICSC - Centro Nazionale di Ricerca in High Performance Computing, Big Data e Quantum Computing, Via Magnanelli 2, Bologna, Italy

<sup>6</sup> Dipartimento di Fisica – Sezione di Astronomia, Università di Trieste, Via Tiepolo 11, Trieste, 34131, Italy

March 18, 2025

## ABSTRACT

Ongoing and upcoming wide-field surveys at different wavelengths will measure the distribution of galaxy clusters with unprecedented precision, demanding accurate models for the two-point correlation function (2PCF) covariance. In this work, we assess a semi-analytical framework for the cluster 2PCF covariance that employs three nuisance parameters to account for non-Poissonian shot noise, residual uncertainties in the halo bias model, and subleading noise terms. We calibrate these parameters on a suite of fast approximate simulations generated by PINOCCHIO as well as full  $N$ -body simulations from OpenGADGET3. We demonstrate that PINOCCHIO can reproduce the 2PCF covariance measured in OpenGADGET3 at the few percent level, provided the mass functions are carefully rescaled. Resolution tests confirm that high particle counts are necessary to capture shot-noise corrections, especially at high redshifts. We perform the parameter calibration across multiple cosmological models, showing that one of the nuisance parameters, the non-Poissonian shot-noise correction  $\alpha$ , depends mildly on the amplitude of matter fluctuations  $\sigma_8$ . In contrast, the remaining two parameters,  $\beta$  controlling the bias correction and  $\gamma$  controlling the secondary shot-noise correction, exhibit more significant variation with redshift and halo mass. Overall, our results underscore the importance of calibrating covariance models on realistic mock catalogs that replicate the selection function of forthcoming surveys and highlight that approximate methods, when properly tuned, can effectively complement full  $N$ -body simulations for precision cluster cosmology.

**Key words.** galaxies: clusters: general / cosmology: theory / large-scale structure of Universe

## 1. Introduction

Galaxy clusters, being the most massive virialized objects in the Universe, have long been recognized as powerful probes of cosmology, thanks to their sensitivity to both the geometry and growth of large-scale structure (see, e.g., Allen et al. 2011; Kravtsov & Borgani 2012). Traditional cluster studies have focused on the abundance of these systems and their variation with redshift to constrain cosmological parameters such as the matter density parameter  $\Omega_m$  and the amplitude of matter fluctuations  $\sigma_8$  (Borgani et al. 2001; Vikhlinin et al. 2009; Planck Collaboration XX: Ade et al. 2014; Planck Collaboration XXIV: Ade et al. 2016; Bocquet et al. 2019; Costanzi et al. 2021). Nonetheless, the two-point correlation function (2PCF) of clusters is also a promising probe, as it is highly sensitive to the bias–mass relation and can help to break degeneracies that affect cluster abundance studies (Schuecker et al. 2003; Majumdar & Mohr 2004; Sartoris et al. 2016; Marulli et al. 2018; Fumagalli et al. 2024). When the 2PCF is combined with other observables such as number counts or weak lensing, it can provide tighter cosmological constraints while helping to calibrate mass–observable relations (Mana et al. 2013; To et al. 2021; Castro et al. 2020).

An accurate assessment of cosmological constraints from cluster clustering hinges on a robust model for the covariance of

the 2PCF. In contrast to the comparatively simpler case of cluster number counts (e.g., Hu & Kravtsov 2003; Fumagalli et al. 2021), the covariance of the 2PCF of clusters requires additional parameters to reproduce the results of numerical simulations, due to non-Gaussianities and non-linearities (Euclid Collaboration: Fumagalli et al. 2024). Recent works have demonstrated that, for photometrically selected cluster surveys similar to the one anticipated from Euclid (Laureijs et al. 2011), a Gaussian model with standard Poisson noise can fail to capture all relevant contributions in the covariance. Consequently, one must introduce ad hoc corrections, calibrated against simulations, that take into account non-Gaussian effects and the specific statistical weight of cluster samples.

In previous studies, fast approximate simulations such as those produced by the PINOCCHIO algorithm (Monaco et al. 2002, 2013; Munari et al. 2017) have proven valuable for modeling the 2PCF covariance. By generating a large number of past-light-cone realizations, it is possible to calibrate the extra parameters associated with the analytical covariance to match measurements from mock cluster catalogs (e.g., Fumagalli et al. 2022). In Euclid Collaboration: Fumagalli et al. (2024), such calibrations were carried out at fixed cosmology, thus leaving the question of whether the best-fit parameters for the covariance depend on the underlying cosmological model open. Moreover, although approximate methods like PINOCCHIO can reproduce many large-scale structure statistics with remarkable efficiency,

\* e-mail: a.fumagalli@physik.uni-muenchen.de

\*\* e-mail: tiago.batalha@inaf.it

they inevitably involve simplifying assumptions in treating non-linear gravitational collapse. It is, therefore, crucial to establish whether the covariance parameters calibrated on PINOCCHIO differ significantly from those obtained from full  $N$ -body simulations.

Among the forthcoming wide-field surveys, the Vera C. Rubin Observatory’s Legacy Survey of Space and Time (LSST)<sup>1</sup> (Abell et al. 2009), the third generation of the South Pole Telescope (SPT-3G)<sup>2</sup> (Benson et al. 2014), eROSITA<sup>3</sup> (Predehl et al. 2021), the Square Kilometre Array (SKA)<sup>4</sup> (Maartens et al. 2015), the Dark Energy Spectroscopic Instrument (DESI)<sup>5</sup> (Aghamousa et al. 2016), the Nancy Grace Roman Space Telescope<sup>6</sup> (Spergel et al. 2015), and *Euclid*<sup>7</sup> (Euclid Collaboration: Mellier et al. 2024), are poised to deliver measurements of summary statistics of the distribution of galaxy clusters with unprecedented statistical precision. These data sets will demand more accurate covariance models to exploit the cosmological information encoded in cluster clustering fully. The goal of this paper is, therefore, twofold. First, we investigate the cosmology dependence of the calibrated parameters that enter the covariance model for the cluster 2PCF. Second, we compare the parameters extracted from PINOCCHIO-based mocks with those calibrated on higher-fidelity  $N$ -body simulations. This analysis directly tests the robustness of the covariance modeling for future surveys such as *Euclid*, which is expected to deliver a photometric cluster catalog of unprecedented size and redshift coverage. Ultimately, a more reliable covariance prescription will improve cosmological constraints from cluster clustering and deepen our understanding of systematic uncertainties.

This paper is structured as follows. In Sect. 2, we present the theoretical framework for the 2PCF, the semi-analytical covariance model, and the procedure for fitting parameters. In Sect. 3, we summarize the simulations used for our covariance calibration and introduce the cluster catalogs derived from PINOCCHIO and  $N$ -body simulations. We compare and discuss our results in Sect. 4, where we quantify the impact of cosmology dependence and the differences between approximate and full  $N$ -body calibrations. We discuss the implications of our results in Sect. 5. Finally, we draw our conclusions in Sect. 6, emphasizing the implications of our findings for the cosmological exploitation of cluster clustering in forthcoming wide-field surveys.

## 2. Covariance formalism

This section concisely summarizes the semi-analytical model for the real-space 2PCF covariance of galaxy clusters (or halos). A more extensive derivation and validation can be found in Meiksin & White (1999) and Euclid Collaboration: Fumagalli et al. (2024), with additional details on numerical calibrations provided by Fumagalli et al. (2022).

### 2.1. Baseline Model and Notation

The core of the 2PCF covariance model starts from the halo power spectrum covariance in Fourier space, which contains both Gaussian and non-Gaussian contributions (see, e.g.,

Meiksin & White 1999; Scoccimarro et al. 1999). In real space, the halo 2PCF at a given redshift  $z$  and separation  $r$  can be expressed as

$$\xi_h(r, z) = \int \frac{k^2 dk}{2\pi^2} P_h(k, z) j_0(kr), \quad (1)$$

where  $P_h(k, z)$  is the halo power spectrum, and  $j_0$  is the spherical Bessel function of order zero. On large (linear) scales, the halo power spectrum can be approximated by

$$P_h(k, z) = \bar{b}^2(z) P_m(k, z) \quad (2)$$

where  $\bar{b}(z)$  is the effective linear bias of halos obtained by averaging the linear bias model presented in Euclid Collaboration: Castro et al. (2024) weighting it by mass according to the halo mass function (HMF; Euclid Collaboration: Castro et al. 2023), and  $P_m(k, z)$  is the linear matter power spectrum. When calculating the covariance, the discrete nature of halos introduces an additional source of randomness that is independent of the clustering of the matter field. This effect, known as shot-noise, is accounted for by adding a  $1/\bar{n}(z)$  term to the power spectrum of Eq. (2). Such a term provides the leading-order Poisson shot-noise component for a point distribution whose redshift-dependent comoving mean number density is  $\bar{n}(z)$ . When transforming to configuration space and integrating over redshift bins, one obtains a baseline (Gaussian + lowest-order shot-noise) model for the 2PCF covariance (cf. Cohn 2006; Hu & Kravtsov 2003):

$$C_{ij}(z) = \frac{2}{V_z} \int \frac{k^2 dk}{2\pi^2} \left[ P_h(k, z) + \frac{1}{\bar{n}(z)} \right]^2 W_i(k) W_j(k) + \frac{2}{V_z} \int \frac{dk k^2}{2\pi^2} \bar{b}^2 P_m(k) \left[ \frac{1}{\bar{n}(z)} \right]^2 W_j(k) \frac{\delta_{ij}}{V_i}. \quad (3)$$

Here  $V_z$  is the comoving volume in the redshift slice,  $W_i(k)$  is the window function for the  $i$ -th separation bin, and the sub-leading terms account for additional shot-noise corrections. In principle, one can include contributions from higher-order correlation terms (Meiksin & White 1999; Scoccimarro et al. 1999) and from super-sample covariance (Takada & Hu 2013) for more accuracy, but they often add significant complexity and require the calibration of nuisance parameters.

### 2.2. Limitations of the Baseline Model

Equation (3) was shown to underestimate the total covariance when compared to simulations (see, for instance, Euclid Collaboration: Fumagalli et al. 2024). Known limitations include:

- **Non-Poissonian Shot Noise:** The simple  $1/\bar{n}$  term in general does not capture the non-Poissonian nature of the sampling of the underlying density field provided by the biased halo distribution, especially at high masses or high redshifts;
- **Inaccurate Bias Prescription:** Linear bias formulae sometimes introduce residual offsets in amplitude or scale dependence;
- **Neglected Higher-Order Terms:** Bispectrum and trispectrum contributions can be non-negligible for cluster-scale halos, particularly if the survey volume or mass threshold is such that the number density is small.

These effects can lead to a mismatch of up to tens of per cent between the baseline model and numerical simulations (Euclid Collaboration: Fumagalli et al. 2024).

<sup>1</sup> <https://www.lsst.org>

<sup>2</sup> <https://astro.fnal.gov/science/cmbr/spt-3g/>

<sup>3</sup> <https://www.mpe.mpg.de/eROSITA>

<sup>4</sup> <https://www.skatelescope.org>

<sup>5</sup> <https://www.desi.lbl.gov>

<sup>6</sup> <https://roman.gsfc.nasa.gov>

<sup>7</sup> <https://www.euclid-ec.org>

The halo bias and shot-noise terms in the covariance can be rescaled by empirical parameters that effectively absorb the missing (or inaccurately modeled) contributions to correct for these discrepancies. In practice, one modifies Eq. (3) as:

$$C_{ij}^{\text{fit}}(z) = \frac{2}{V_z} \int \frac{k^2 dk}{2\pi^2} \left[ (\beta \bar{b})^2 P_m(k, z) + (1 + \alpha) \frac{1}{\bar{n}(z)} \right]^2 W_i(k) W_j(k) + \frac{2}{V_z} \int \frac{dk k^2}{2\pi^2} (\beta \bar{b})^2 P_m(k) \left[ (1 + \gamma) \frac{1}{\bar{n}(z)} \right]^2 W_j(k) \frac{\delta_{ij}}{V_i}, \quad (4)$$

where  $\alpha$ ,  $\beta$ , and  $\gamma$  are treated as nuisance parameters to be calibrated against a suite of mock halo catalogs extracted from simulations. In summary,

- $\beta$  corrects for residual bias errors (i.e., an over- or underestimation of  $\bar{b}$ ),
- $\alpha$  adjusts the main shot-noise amplitude to account for non-Poissonian behavior and missing non-Gaussian terms,
- $\gamma$  modifies a secondary shot-noise contribution in the diagonal terms, mostly contributing at small scales.

By fitting  $\{\alpha, \beta, \gamma\}$  to simulation measurements, one can achieve better than 10 percent agreement between the analytical covariance and the fully numerical result, at least for a fixed cosmology (Euclid Collaboration: Fumagalli et al. 2024).

### 2.3. Fitting procedure

The fitting method, presented in Fumagalli et al. (2022), is designed to efficiently construct a reliable covariance matrix by constraining a model with free parameters. The procedure begins by defining a model covariance matrix, which may be incomplete or approximate, and introducing free parameters to capture unknown or uncertain contributions to the covariance. The model is then constrained by maximizing a Gaussian likelihood function evaluated at a fixed fiducial cosmology, with the free parameters of the covariance matrix as fitting variables. The best-fit covariance is then obtained by ensuring that the  $\chi^2$  values from the model match the theoretical distribution for the observed data: the correct covariance should provide  $\chi^2$  values from each simulation that follow a  $\chi^2$  distribution. The key advantage of this approach is that it requires significantly fewer simulations than traditional methods for covariance estimation—typically around  $10^2$  simulations, compared to the thousands ( $\sim 10^3 - 10^4$ ) usually needed for a full, accurate numerical covariance matrix.

## 3. Methodology

We generate halo catalogs using two different approaches: large  $N$ -body simulations with OpenGADGET3 and approximate simulations with PINOCCHIO. Below, we describe the setup of each simulation suite, summarize the resulting halo catalogs used in our analyses, and describe the procedure to measure the 2PCF and power spectra.

### 3.1. $N$ -body simulations

$N$ -body simulations are carried out with the Tree-PM OpenGADGET3  $N$ -body code (Dolag et al. in prep.). OpenGADGET3 represents an evolution of the GADGET3 code, which in turn provides an improvement of the publicly available GADGET2 code (Springel 2005). It adopts a mixed MPI/OpenMP

**Table 1.** The different cosmological parameters considered in this work.

Name	$\Omega_{m,0}$	$h$	$\Omega_{b,0}$	$n_s$	$\sigma_8$
C0	0.3158	0.6732	0.0494	0.9661	0.8102
C1	0.1986	0.7267	0.0389	0.9775	0.8590
C2	0.1665	0.7066	0.0417	0.9461	0.8341
C3	0.3750	0.6177	0.0625	0.9778	0.7136
C4	0.3673	0.6353	0.0519	0.9998	0.7121
C5	0.1908	0.6507	0.0527	0.9908	0.8971
C6	0.2401	0.8087	0.0357	0.9475	0.8036
C7	0.3020	0.5514	0.0674	0.9545	0.8163
C8	0.4093	0.7080	0.0446	0.9791	0.7253

**Notes.** The cosmological parameters have been uniformly drawn from the 95 percent confidence level hyper-volume of the cluster abundance constraints presented in Costanzi et al. (2021).

parallelization that allows the code to optimally exploit the parallelism offered by computing nodes with a significant amount of shared memory. Our simulations adopt a flat  $\Lambda$ CDM cosmology that we refer to as C0 throughout this paper and present the specific cosmological parameter values in Table 1.

We run 120 realizations of this cosmology, each following  $2048^3$  dark matter particles in a comoving, cubic box of side length  $3870 h^{-1}$  Mpc. The gravitational softening length is chosen to be one-fortieth of the mean inter-particle spacing, ensuring that the halo mass function and large-scale clustering are well-resolved across the range of halo masses of interest (typically  $M \gtrsim 10^{14} h^{-1} M_\odot$ ). The initial conditions (ICs) for 100 of these realizations are generated with the MONOFONIC code (Michaux et al. 2021). The remaining 20 adopt the same Fourier amplitudes and phases used for a subset of the PINOCCHIO simulations (see Sect. 3.2) to facilitate a direct comparison.

Each OpenGADGET3 simulation is evolved from  $z = 24$  down to  $z = 0$ , outputting snapshots at various intermediate redshifts  $z \in \{0.0, 0.5, 1.0, 2.0\}$ . We identify halos in each snapshot using SUBFIND (Springel et al. 2001; Dolag et al. 2009; Springel et al. 2021). SUBFIND determines halos by first executing a parallel friends-of-friends with linking length set to 0.2 (FOF, see, Davis et al. 1985, for instance) and then assigning its center to the position of the particle with the lowest potential. The simulation outputs provide a set of *comoving box* halo catalogs for each realization.

### 3.2. Approximate simulations: PINOCCHIO

We also use the Lagrangian Perturbation Theory (LPT)-based PINOCCHIO code (Monaco et al. 2002, 2013; Munari et al. 2017) to produce halo catalogs in a more computationally efficient manner, enabling exploration of multiple cosmological models and a large number of realizations.

This work complements the original set of PINOCCHIO catalogs presented in Fumagalli et al. (2021) and serves as a basis for comparison. We generate 20 PINOCCHIO realizations using the C0 cosmological parameters and the same mass resolution as our OpenGADGET3 simulations. These runs employ identical box size, particle number ( $2048^3$ ), and initial Fourier mode amplitudes and phases, enabling a direct one-to-one comparison of halo statistics between PINOCCHIO and full  $N$ -body catalogs under identical initial conditions. In contrast, the original set assumed  $\Omega_{m,0} = 0.30711$  and used a grid of  $2160^3$  elements, which led to a mass resolution difference of roughly 20 percent.

We further exploit PINOCCHIO efficiency to create an extensive suite of 900 comoving box simulations covering nine



additional cosmological models, labeled originally C0 through C8 in [Euclid Collaboration: Castro et al. \(2023\)](#). Each cosmology has 100 realizations, each with  $3072^3$  dark matter particles in a box the same size as the previously presented simulations. These simulations broadly sample parameter space, enabling us to study how our covariance model (and its nuisance parameters) might vary across different cosmological parameters.

In addition to comoving outputs, PINOCCHIO can generate halo catalogs on past light cones. We construct such cones with a 60 deg aperture. These light-cone catalogs mimic in a simplistic way the typical sky coverage of future wide-field cluster survey footprints on an idealized uniform and unmasked coverage.

### 3.3. Summary of simulation sets

Overall, we have assembled:

1. 900 high-resolution PINOCCHIO realizations spanning nine distinct cosmological models (C0–C8), each with  $3072^3$  particles and box size of  $3870 h^{-1}$  Mpc, for robust exploration of cosmology dependence. We further generated catalogs in the past light cone of 60 deg aperture for these simulations, mimicking wide-field cluster surveys;
2. 100 low-resolution  $N$ -body realizations at the C0 cosmology with the same box size and  $2048^3$  particles;
3. 20 PINOCCHIO and 20  $N$ -body realizations were generated at low resolution ( $2048^3$  particles) assuming the C0 cosmology. Both simulations employed identical phases and amplitudes of the initial Fourier modes, thereby allowing straightforward comparisons of halo statistics within comoving boxes of identical size. Because the PINOCCHIO and OpenGADGET3 runs in this sub-set share the same initial conditions, the sample noise in the relative statistics between the two codes is greatly reduced;
4. 100 PINOCCHIO realizations from the set used in [Fumagalli et al. \(2021\)](#); [Euclid Collaboration: Fumagalli et al. \(2024\)](#), with low resolution similar to the  $N$ -body set. These mocks, labeled as “original” set, have the same box size and a cosmology similar to C0. This last set will serve as a reference for comparison with previous works.

The combination of full  $N$ -body and approximate PINOCCHIO simulations at matched initial conditions and over multiple cosmologies allows us to assess the robustness of the 2PCF covariance model, as well as the cosmology dependence of the nuisance parameters introduced in Sect. 2.

### 3.4. Post-Processing

#### 3.4.1. Mass rescaling

PINOCCHIO has been calibrated to reproduce within a few percent the FOF-based HMF presented by [Watson et al. \(2013\)](#). To reproduce instead our adopted model for the HMF ([Euclid Collaboration: Castro et al. 2023](#)) while keeping the sample variance and shot-noise for each simulation, we implement the rescaling of the halo masses as proposed by [Fumagalli et al. \(2021\)](#) on all PINOCCHIO outputs. In order to obtain a fair comparison in Sect. 4.1, we also rescale the original set of PINOCCHIO mocks to the [Euclid Collaboration: Castro et al. \(2023\)](#) HMF. The same procedure was applied to the OpenGADGET3 halo catalogs to keep consistency between the catalogs. Given the proven accuracy of our fiducial HMF calibration presented in [Euclid Collaboration: Castro et al. \(2023\)](#), the impact of the recalibration for the  $N$ -body simulation is rather small.

#### 3.4.2. Power-Spectra

We used the set of **PY**thon **L**ibraries for the **A**nalysis of **N**umerical **S**imulations (PYLIANS)<sup>8</sup> to construct the density field and compute the power spectra from the halo catalogs. For the 20 simulations that share the initial conditions between OpenGADGET3 and PINOCCHIO, the cross-spectra between matter and halos are calculated using the linear density field produced by PINOCCHIO. All power spectra were calculated from a 3D grid with  $512^3$  mesh points on which the density traced by the halo distribution is assigned with a Cloud In Cell (CIC) scheme. The power-spectra measurements are averaged within shells in  $k$ -space with widths given by  $k_f \equiv 2\pi/L$ , corresponding to the fundamental mode of the box.

#### 3.4.3. 2PCF

We measure the 2PCF by comparing halo pair distributions in the data and random catalogs using the estimator from [Landy & Szalay \(1993\)](#). The random catalog is created by extracting and shuffling positions of a subset of halos from each mock catalog, generating a catalog with  $n_R = 20 n_D$  objects, randomly distributed within the box/lightcone volume.

The 2PCF is computed for halos with masses above  $10^{14} h^{-1} M_\odot$  and  $3 \times 10^{14} h^{-1} M_\odot$ , in 25 log-spaced bins in the separation range  $r = 20 - 130 h^{-1}$  Mpc, which includes linear scales, where the bias is almost constant, and the BAO peak. As for the analysis of the lightcones, we consider four redshift bins of width  $\Delta z = 0.5$  in the range  $z = 0 - 2$ . The pair counts in the data-data, data-random, and random-random catalogs are measured using the CosmoBolognaLib package ([Marulli et al. 2016](#)).

## 4. Results

This section provides a systematic comparison of the 2PCF and its covariance measured from the simulation sets introduced in Sect. 3. We assess resolution effects in PINOCCHIO (Sect. 4.1), comparing C0 simulations from “set 1” to original simulations in “set 4”, as well as PINOCCHIO simulations in “set 3”. Next, we directly compare PINOCCHIO and OpenGADGET3 simulations with identical initial conditions (“set 3”, Sect. 4.2), quantifying the agreement in bias and shot-noise corrections, as well as in the covariance parameters fitted from “set 1” and “set 2”. Finally, we examine the cosmology dependence of the covariance-model parameters (Sect. 4.3), using all the “set 1” simulations.

### 4.1. Resolution

In Fig. 1, we present a comparison between the 2PCF measurement at redshifts  $z = 0$  and  $z = 1$  for the high-resolution C0 PINOCCHIO simulations (“set 1”) and the low-resolution original set (“set 4”). The cosmological parameters from the original simulations and the C0 ones differ. Still, the difference in the theoretical expectation is too small to be seen on the logarithmic scale, and therefore, we present it only for the C0 case. In the bottom panel, we present the residual between the measurements and the corresponding theoretical measurements. We observe similar trends between the simulation sets at both redshifts. At redshift  $z = 0.0$ , PINOCCHIO reproduces the theoretical expectation within 10 percent for the range of separation  $r \in (35 - 115) h^{-1}$  Mpc. The agreement between PINOCCHIO

<sup>8</sup> <https://github.com/franciscovillaescusa/Pylians>

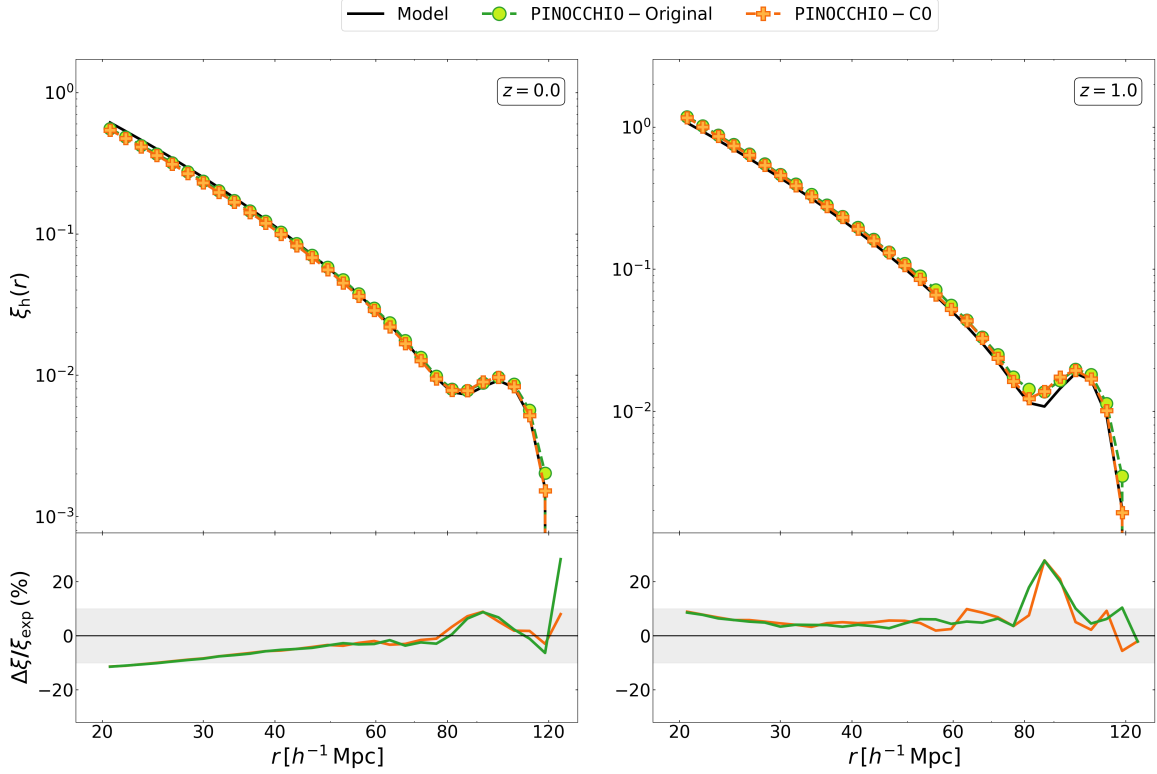


**Fig. 1.** *Top:* Comparison of the PINOCCHIO 2PCF measured on the comoving box from the original mocks (Fumagalli et al. 2021) and our new high-resolution C0. The new and original simulations assume different but similar cosmologies. We present only the theoretical expectation for the C0 cosmology for better figure readability. *Bottom:* residual between the measured 2PCF and the respective theoretical expectation. The shaded gray area denotes the region within a relative difference smaller than 10 per cent.

and expectations generally improves for the case  $z = 1.0$ . Still, we notice that in the region  $r \sim 85 h^{-1} \text{ Mpc}$  the agreement worsens. This fluctuation is due to the binning where the steepness of the 2PCF close to the BAO peak causes an artificially large impact. In the residual panel of Fig. 1, we observe that the new and original sets present similar behaviors, ruling out possible resolution effects from the original calibration.

Similarly to Fig. 1, in Fig. 2, we compare the baseline 2PCF covariance presented in Eq. (3) between the original set and the C0 subset. We present the results for the diagonal (darker colors) and first off-diagonal terms (lighter colors). The similar behavior between the original and new simulations, which have higher resolution, confirms the claim of Euclid Collaboration: Fumagalli et al. (2024) that the baseline model cannot account for the observed covariance in simulations without calibration of the parameters  $\alpha$ ,  $\beta$ , and  $\gamma$ .

To assess the impact of the resolution on the PINOCCHIO predictions, in Fig. 3, we compare the bias  $b$  and shot-noise correction  $\alpha$  measured from the new 100 C0 simulations at higher resolution with respect to the 20 simulations with same cosmology but lower resolution. The measurements are from the outputs in comoving boxes at different redshifts and with different minimum mass selection  $M_{\text{cut}} \in \{10^{14}, 3 \times 10^{14}\} M_{\odot} h^{-1}$ . We measured the bias from the ratio of the cross-spectrum  $P_{h,m}$  between the halo and matter to the matter-power spectrum  $P_m$ . The shot-noise correction  $\alpha$  is measured using the following relation

$$\alpha(k) + 1 = \bar{n}(z) \left( P_h(k, z) - \frac{P_{h,m}(k, z)^2}{P_m(k, z)} \right), \quad (5)$$

where  $\bar{n}(z)$  is the mean density of halos.

We observe in Fig. 3 that the differences in the bias due to resolution are more minor than 2 percent for the different mass and redshift selections, except the redshift two, where differences are roughly 5 percent for  $10^{14} M_{\odot} h^{-1}$  mass selection. The case for the mass selection of  $3 \times 10^{14} M_{\odot} h^{-1}$  is not shown for redshift two as, in this case, the measurements are very noisy due to the small number of tracers. Concerning the shot-noise correction  $\alpha$ , we observe that the original simulations converge within a few percent for redshifts below unity. For redshift  $z = 1$ , while the measurements from the  $10^{14} M_{\odot} h^{-1}$  still agree within said accuracy, for the  $3 \times 10^{14} M_{\odot} h^{-1}$ , we observe a difference of the order of 10 percent. The differences can be as significant as 30 percent for the case of redshift  $z = 2$ . This indicates that the original resolution might be too low to calibrate the shot-noise correction accurately at high redshift.

Notice that the parameters  $\alpha$  and  $\beta$  in the covariance model have slightly different meanings and values compared to those fitted from the power spectrum. This is because the three covariance parameters also absorb the effects of missing higher-order terms in the covariance, partially losing their physical interpretation (Euclid Collaboration: Fumagalli et al. 2024). The agreement between these parameters will be discussed in Sect. 4.2.1.

#### 4.2. OpenGADGET3 vs PINOCCHIO

In Fig. 4, we compare the effective halo bias measured from the mass-scaled catalogs produced by OpenGADGET3 and

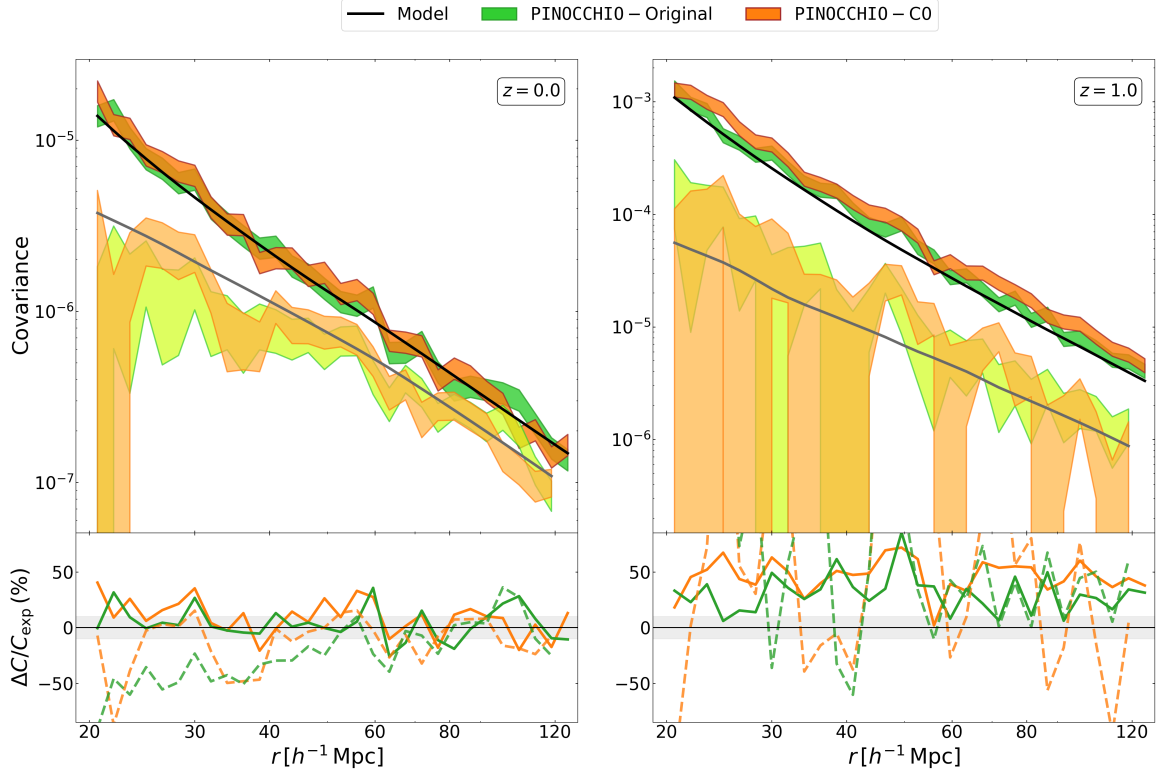


**Fig. 2.** *Top:* Comparison of the PINOCCHIO covariance of the 2PCF measured on the comoving box from the original mocks (Fumagalli et al. 2021) and our new high-resolution C0. Similarly to Fig. 1, we present only the theoretical expectation from the baseline model presented in Eq. (3) for the C0 cosmology for better figure readability. *Bottom:* residual between the measured 2PCF and the respective theoretical expectation. In both panels, darker colors are used for diagonal and lighter for the first off-diagonal terms.

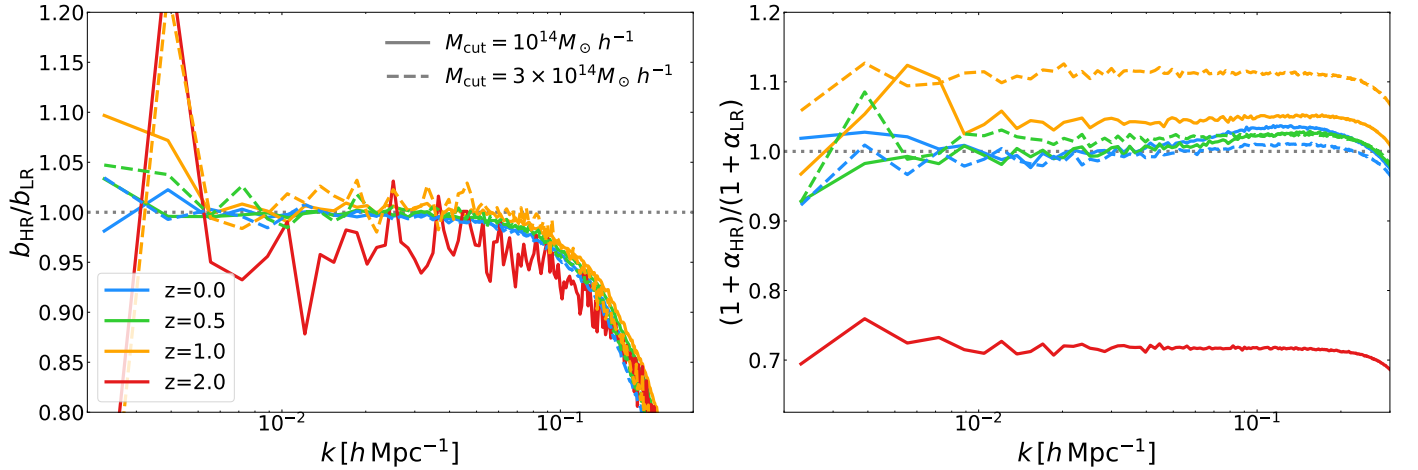


**Fig. 3.** Comparison of resolution effects on PINOCCHIO predictions for halo bias  $b(k)$  (left) and shot-noise correction  $\alpha(k)$  (right). We show the ratio between high-resolution (HR: 100 C0 simulations) and low-resolution (LR: 20 simulations) results at redshifts  $z \in \{0.0, 0.5, 1.0, 2.0\}$  for two mass thresholds:  $M_{\text{cut}} = 10^{14} M_{\odot} h^{-1}$  (solid) and  $M_{\text{cut}} = 3 \times 10^{14} M_{\odot} h^{-1}$  (dashed). While bias differences remain below two percent for  $z \leq 1.0$ , reaching 5 percent at  $z = 2$  (the larger mass cut case is omitted for  $z = 2$  due to noise), the shot-noise corrections converge within 10 percent for  $z \leq 1$  but show 30 percent deviations at  $z = 2$ .

PINOCCHIO (“set 3”) to the theoretical prediction from Euclid Collaboration: Castro et al. (2024). Overall, OpenGADGET3 and PINOCCHIO agree at the 5–10% level for most scales and redshifts, but at higher redshifts (particularly  $z = 2.0$ ) and for larger mass cuts, we observe slightly larger deviations. These differences between the codes reflect residual non-linearities or shot-

noise corrections not fully captured by the mass-scaling procedure.

In Fig. 5, we compare the non-Poissonian correction to the shot noise,  $\alpha(k)$ , for the same halo catalogs. We find that both OpenGADGET3 and PINOCCHIO exhibit broadly similar trends in  $\alpha(k)$ , remaining close to zero for large scales and high redshifts

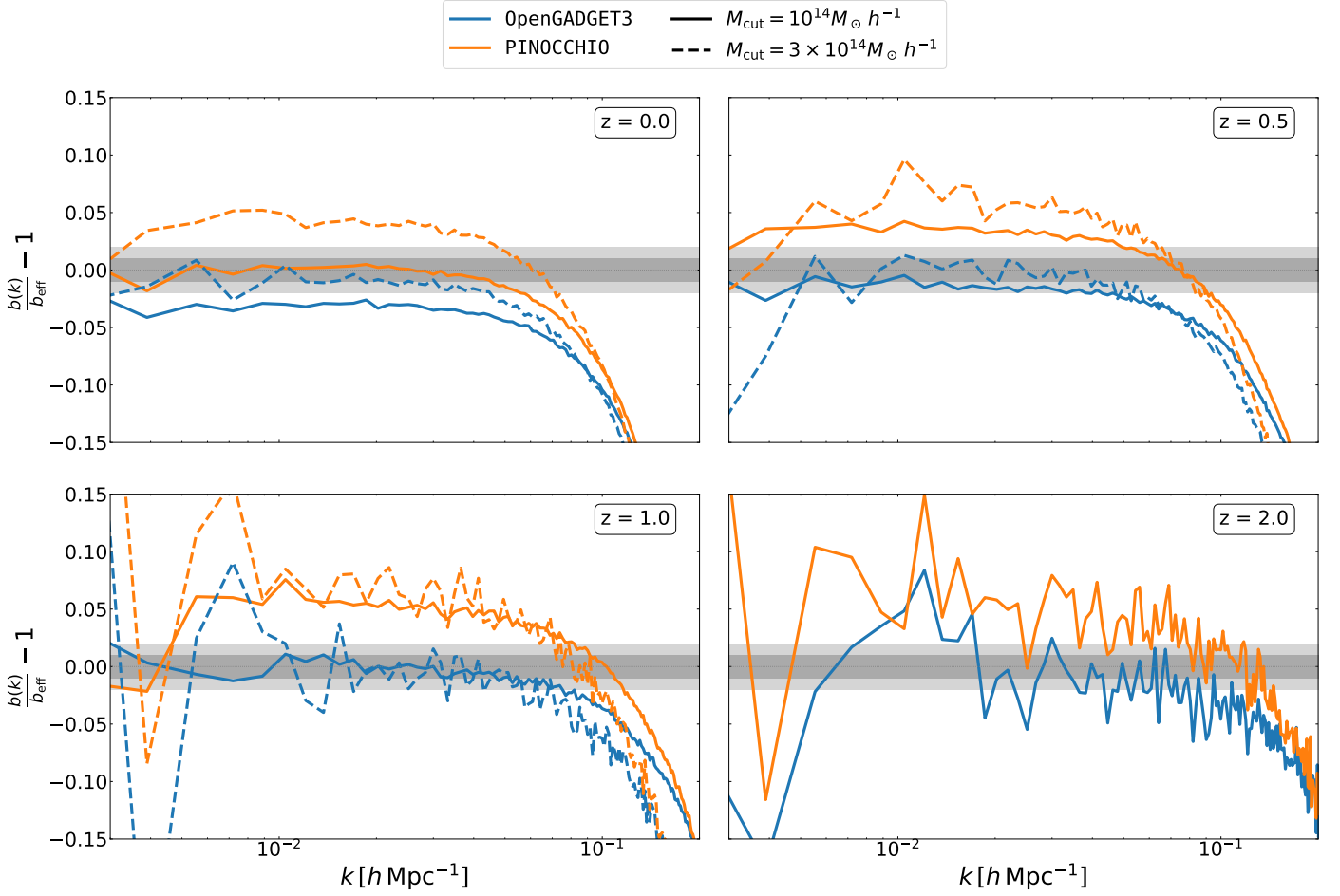


**Fig. 4.** Comparison between the effective bias from mass-scaled halo catalogs from OpenGADGET3 and PINOCCHIO and the theoretical expectation from Euclid Collaboration: Castro et al. (2024). Different panels show the results for different redshifts corresponding to  $\{0.0, 0.5, 1.0, 2.0\}$  clockwise. Different line styles correspond to different minimum mass selections. We omit the result for the  $M_{\text{cut}} = 3 \times 10^{14} h^{-1} M_{\odot}$  at  $z = 2$  as the measurements are too noisy due to the low statistics.

but displaying noticeable deviations for high masses and lower redshifts.

Figures 4 and 5 highlight that, when using the same initial phases and a consistent mass-scaling scheme, OpenGADGET3 and PINOCCHIO reproduce the large-scale bias and shot-noise properties of halo catalogs to within a few percent in most regimes. These results suggest that our mass-scaling procedure effectively aligns the mass functions between OpenGADGET3 and PINOCCHIO. Still, subtle discrepancies remain, likely reflecting that the scaling procedure does not consider each cluster’s environment.

#### 4.2.1. Fits on the Simulation Boxes

Figure 6 presents the posterior distributions of the parameters  $\alpha$ ,  $\beta$ , and  $\gamma$  from Eq. (4), derived by fitting the 2PCF covariance measured in the *comoving boxes* for OpenGADGET3 (“set 2”) and PINOCCHIO (“set 1”).

Overall, we observe good agreement between the two codes for both mass cuts. The values of  $\alpha$  and  $\gamma$  are broadly consistent across the different simulations, reflecting similar levels of non-Poissonian noise corrections and subleading shot-noise contributions. A slight offset emerges in  $\beta$ , with PINOCCHIO typically favoring higher values than OpenGADGET3, in line with the differences in the practical bias seen in Fig. 4. This offset suggests that

the PINOCCHIO halos may require a larger rescaling of the bias to reproduce the measured covariance, possibly reflecting the limitations of the approximated method. Nonetheless, the overlap in the posterior contours for all parameters indicates that the two approaches yield broadly consistent covariance calibrations. Evidence for this can be observed in Fig. 7, which compares the numerical and semi-analytical covariances for OpenGADGET3 and PINOCCHIO, using best-fit parameters from Fig. 6. The residuals between the two models show agreement within 5% in most cases, except for off-diagonal terms at  $z = 1$ . However, these terms are subdominant and do not significantly impact cosmological analysis. Such a result reinforces the conclusion that PINOCCHIO can reliably match OpenGADGET3 covariance results with an appropriate mass-scaling procedure and modest adjustments of the nuisance parameters.

We also find that fitting the covariance parameters using 100 mocks yields stable results up to 25 separation bins within our chosen radial range. Although this is not a universal criterion, more than 100 simulations may be required if a finer binning scheme is used.

#### 4.3. Cosmological dependency

In Fig. 8, we show the best-fit values for the covariance model from Eq.(4) as a function of cosmology. For a more realistic

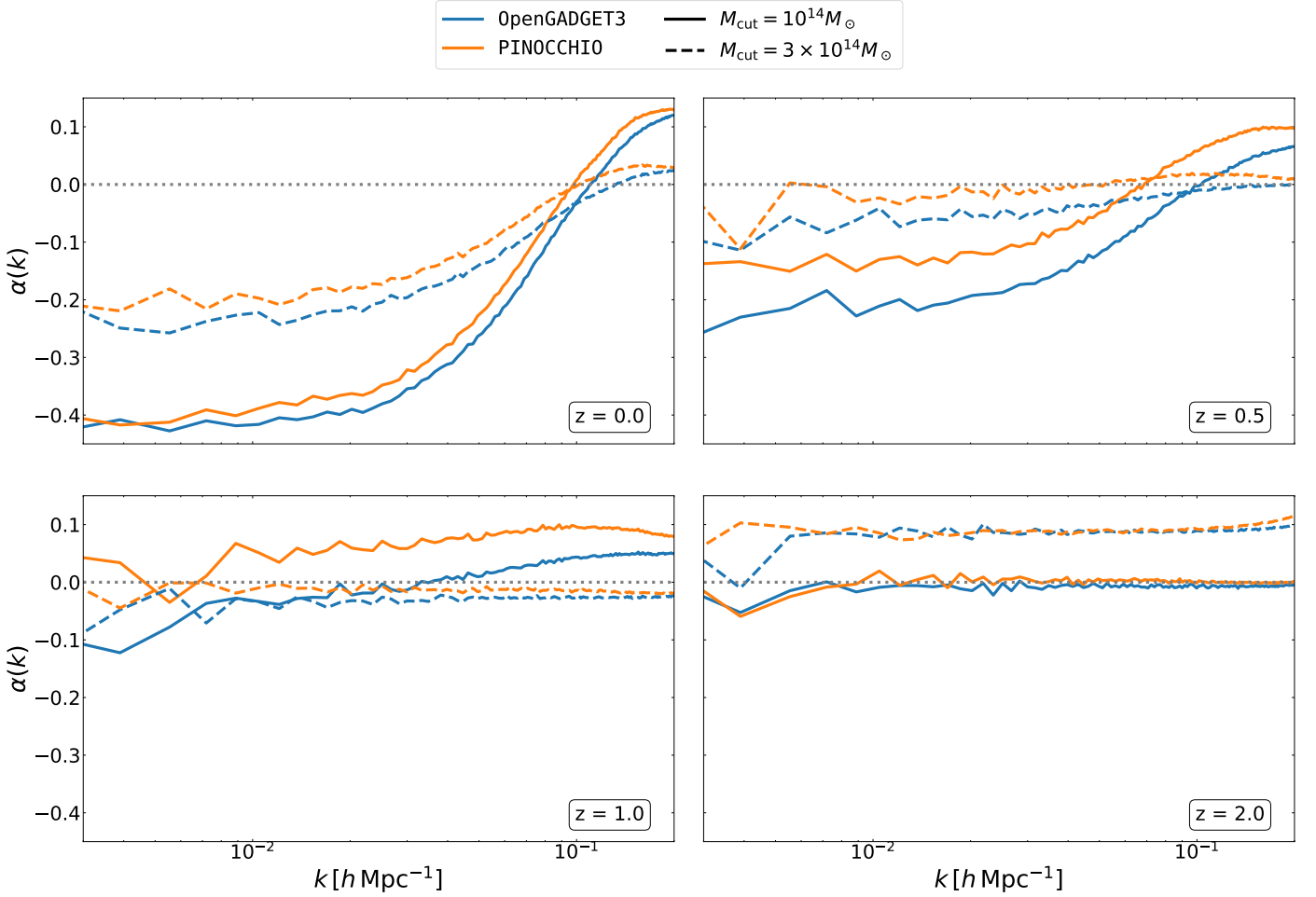


**Fig. 5.** Comparison between the non-Poissonian correction to the shot-noise of the mass-scaled halo catalogs from OpenGADGET3 and PINOCCHIO. Different panels show the results for different redshifts corresponding to  $\{0.0, 0.5, 1.0, 2.0\}$  clockwise. Different lifestyles correspond to different minimum mass selections.

comparison, we perform the fit on lightcones, divided into different redshift bins. The parameter  $\alpha$ , while staying within the range  $[-0.05, 0.15]$ —indicating small deviations from Poissonian shot noise—tends to increase with  $\sigma_8$ , suggesting a mild linear dependence on the amplitude of matter fluctuations. By contrast,  $\beta$  (the bias rescaling) and  $\gamma$  (the sub-leading shot-noise correction) do not show a strong trend with  $\sigma_8$ . However, both  $\beta$  and  $\gamma$  exhibit noticeable variations with redshift. Specifically,  $\beta$  remains in the range  $[1.0, 1.5]$  for the different cosmologies but shifts slightly across redshift bins. At the same time,  $\gamma$  is negative for most cosmologies, implying that the baseline Poisson noise may be an overestimate of the actual sampling noise in specific regimes but tends to decrease with increasing redshift. These results emphasize that even though the global amplitude of non-Poissonian effects and bias corrections is small, allowing for flexible parameters in the covariance model is essential to capture the redshift dependencies and subtle but non-trivial responses to variations in  $\sigma_8$ .

Additionally, the amplitude of  $\beta$  typically exceeds the observed accuracy of PINOCCHIO in reproducing the linear bias, suggesting that  $\beta$  may absorb extra flexibility beyond merely correcting the bias (e.g., mild non-linearities). Furthermore, the redshift dependence of both  $\beta$  and  $\gamma$  indicates that these parameters are sensitive to the survey selection function. Consequently, when applying the model to cosmological data, one should calibrate these parameters on realistic mocks that replicate the actual

selection function, ensuring that the resulting covariance matrix accurately captures both the intrinsic clustering of the sample and the observational selection effects.

Although we show the results for increasing  $\sigma_8$ , we have also analyzed the residual dependency as a function of  $\Omega_m$  and the composite variable  $S_8 = \sigma_8 \sqrt{\Omega_m/0.3}$ . While  $\alpha$  shows some small dependence on  $S_8$ , it is less significant than the dependence on  $\sigma_8$ ; the other parameters do not show any considerable dependency.

The dependency of the non-Poissonian correction primarily on  $\sigma_8$  and not on  $S_8$  is indicative that the clustering amplitude of the underlying density field is the physical mechanism behind it and not the number density of halos of a given mass, which is instead determined by  $S_8$ . Non-linear clustering indeed introduces correlations between the fluctuations in the halo number density that could be reflected in the deviation of the density field sampling provided by halos from a standard Poisson sampling. A thorough study of this issue deserves a dedicated analysis that goes beyond the scope of this work.

## 5. Discussion

Approximate methods, and in the specific case of this paper, the PINOCCHIO code, have become a valuable tool in cosmology by providing results in a fraction of the time required by full  $N$ -body simulations (Chuang et al. 2015; Monaco 2016). However, this



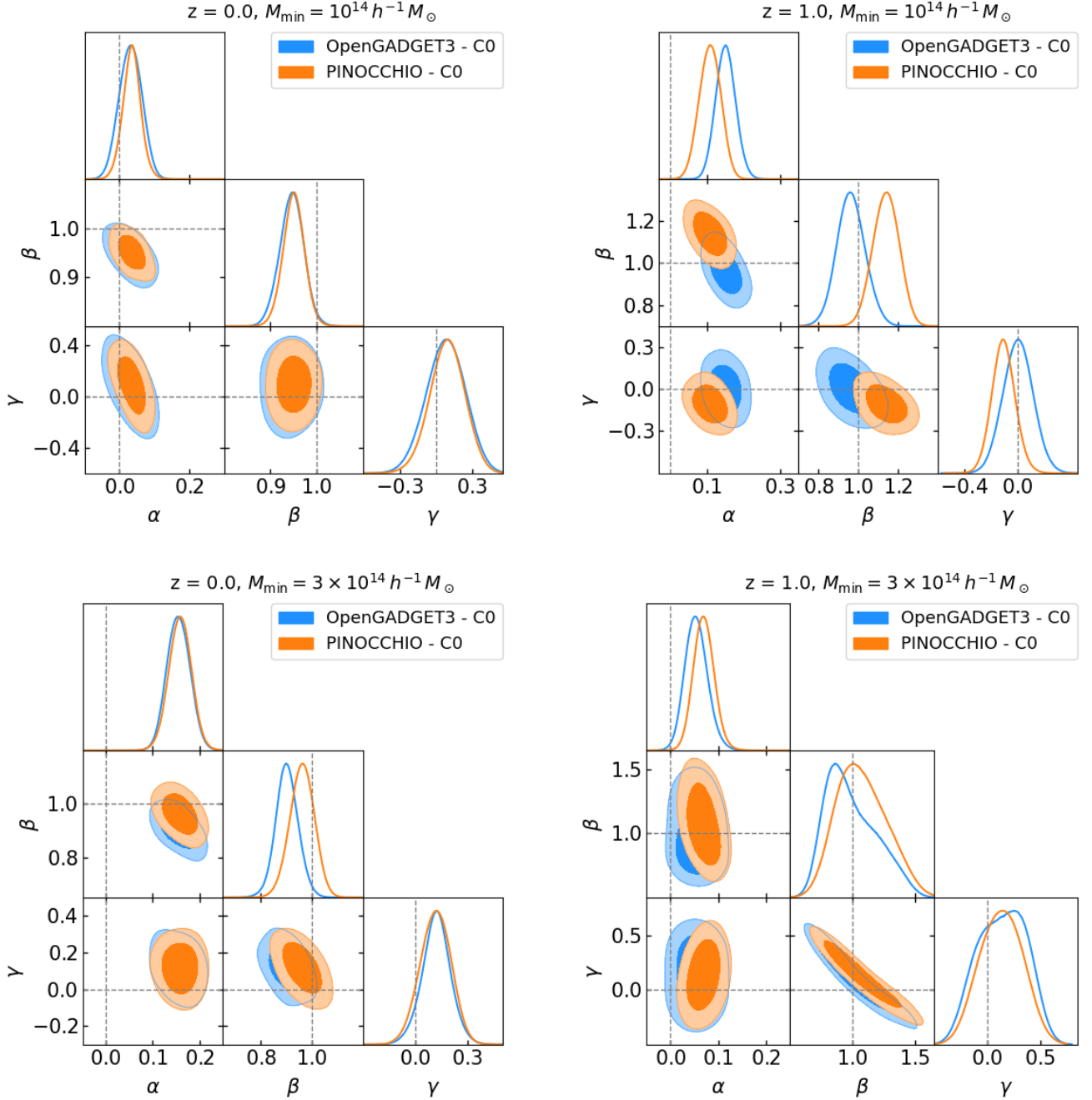


**Fig. 6.** Posteriors for fitted covariance parameters: PINOCCHIO vs OpenGADGET3 for the C0 cosmology. On the *left panels* redshift  $z = 0$ , on the *right panels* redshift  $z = 1$ . *Top panels:*  $M > 10^{14} h^{-1} M_{\odot}$ , *Bottom panels:*  $M > 3 \times 10^{14} h^{-1} M_{\odot}$ .

efficiency is achieved by compromising the accuracy with which the underlying statistical properties are reproduced. Different papers have shown that PINOCCHIO nominal accuracy for different statistics, including subhalo clustering data (Berner et al. 2022) and full-sky 21 cm intensity mapping mocks (Hitz et al. 2024), is roughly 10 percent. Due to its efficiency, PINOCCHIO is a natural candidate to generate massive synthetic data needed to extract the covariance of different cluster statistics numerically (Fumagalli et al. 2021; Euclid Collaboration: Fumagalli et al. 2024). However, as shown by Sellentin & Starck (2019), approximate covariance matrices might bias cosmological constraints and, therefore, should be treated at equal footing with the signal modeling to ensure an unbiased analysis.

In this paper, we have focused on the cluster clustering covariance. In Euclid Collaboration: Fumagalli et al. (2024), it was shown that the low-order analytical model of Meiksin & White (1999) does not quantitatively reproduce the numerical covariance extracted from PINOCCHIO catalogs. Euclid Collaboration: Fumagalli et al. (2024) proposed a semi-analytical extension, presented in Sect. 2. The proposed model could reproduce the covariance accurately if the free parameters  $\alpha$ ,  $\beta$ , and  $\gamma$  appearing in Eq.4 were appropriately calibrated (Fumagalli et al. 2022). Therefore, it is important to assess the resolution, cosmological, and methodological impacts on the calibration of these parameters.

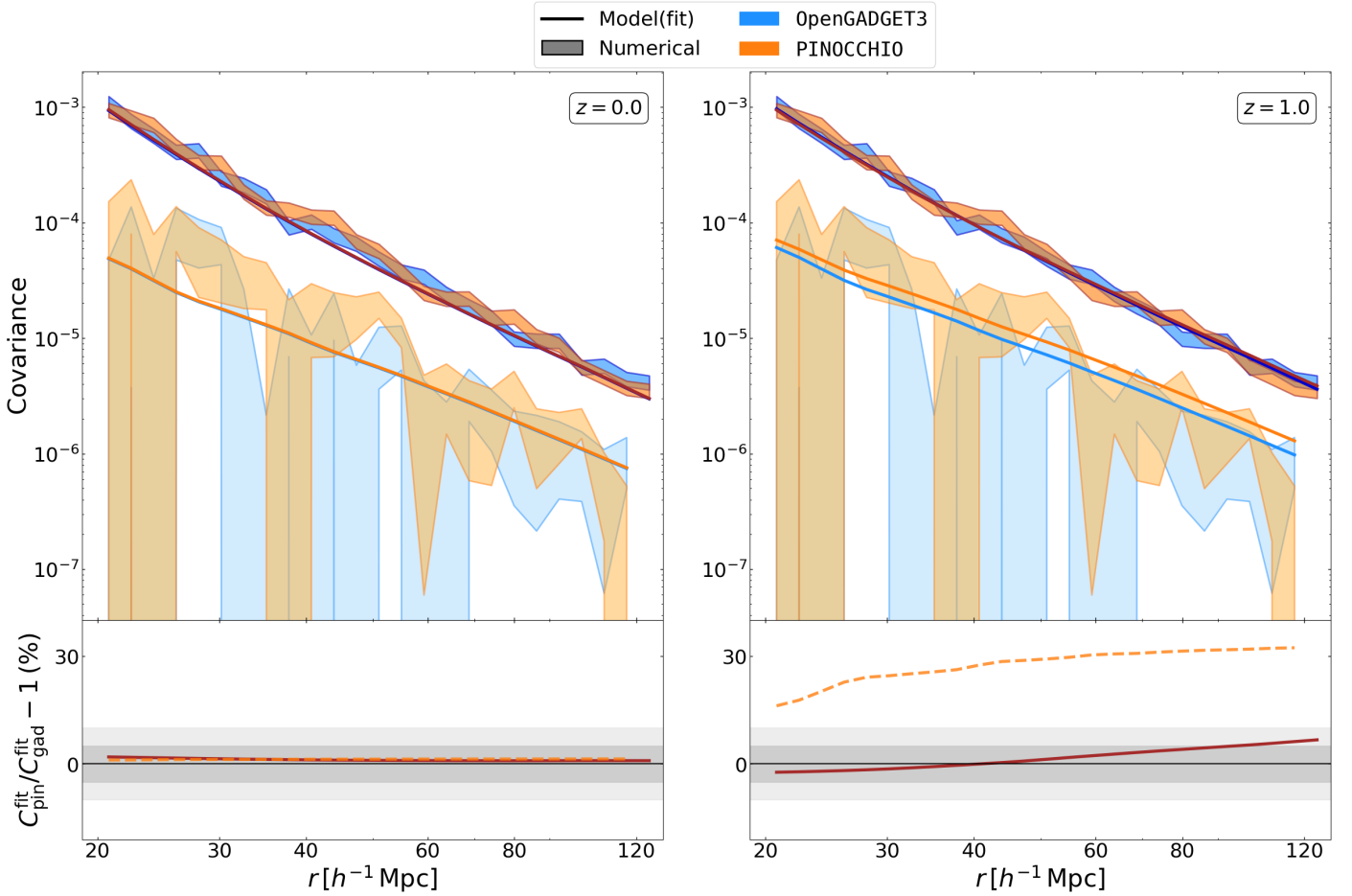


**Fig. 7.** Covariance comparison (box): PINOCCHIO vs OpenGADGET3 covariance matrices, at  $z = 0$  (left panel) and  $z = 1$  (right panel). Shaded areas represent the numerical covariance within  $1\sigma$  uncertainty, and solid lines are the semi-analytical prediction, with fitted parameters. Orange colors indicate PINOCCHIO covariance, while blue colors are for OpenGADGET3 – darker colors represent the diagonal terms, lighter colors are the first off-diagonal terms. Bottom panels show the residuals of the PINOCCHIO fitted model with respect to the OpenGADGET3 one (solid line for the diagonal elements, dashed line for the off-diagonal ones).

The parameters  $\alpha$  and  $\beta$  are related to the shot-noise correction to the Poisson expectation and residual errors on the linear bias. The non-Poissonian correction can be measured from the simulations using the matter, halo, and matter-halo power spectrum using the estimator presented in Eq. (5). The need for a bias correction can be assessed by comparing the halo bias, as measured from the ratio of the matter-halo cross-spectrum and matter power-spectrum at linear scales, concerning the fiducial linear bias model Euclid Collaboration: Castro et al. (2024). In Sect. 4.1, we show that a mass resolution of approximately  $6 \times 10^{11} h^{-1} M_{\odot}$  for PINOCCHIO is too low to produce convergent results for  $\alpha$  and  $\beta$ , especially at higher redshifts, compared to a simulation that has a factor of 4 more resolution elements.

Regarding the comparison between PINOCCHIO and OpenGADGET3, in Sect. 4.2, we show that the shot-noise correction displays similar trends in both codes. However, the overall amplitude of the shot-noise correction (i.e.,  $1 + \alpha$ ) differs by as much as 10 percent. In contrast, for the bias correction  $\beta$ , PINOCCHIO systematically overpredicts the value relative to OpenGADGET3, with a stable relative difference of approximately 5 percent that could be easily corrected during calibration. Correcting this slight bias would yield an even better agreement between the calibrations of PINOCCHIO and OpenGADGET3. Nevertheless, even without such a correction,

the covariances obtained from both codes remain statistically equivalent within the uncertainties assessed in this work.

Furthermore, regarding the cosmological dependency of the parameters, only  $\alpha$  shows a small dependency with  $\sigma_8$ . While the linear coefficients of said relation do not show a redshift dependency, its normalization decreases with redshift over the redshift range  $z = [0-1]$  and is constant at larger redshift.

Lastly, for both PINOCCHIO and OpenGADGET3 we observe that the extra parameters  $\alpha$ ,  $\beta$ , and  $\gamma$  depend on redshift and mass cuts. This dependency implies that the final covariance depends on the selection function. Therefore, future cosmological analysis should use mock catalogs that mimic the sample selection function.

## 6. Conclusions

In this paper, we have assessed the robustness of the calibration of the semi-analytical model for the 2PCF covariance on both fast approximate PINOCCHIO and OpenGADGET3  $N$ -body simulations across multiple cosmological models. We summarize our main findings:

- The shot-noise corrections and bias calibration converge more reliably in higher-resolution PINOCCHIO simulations ( $M_{\text{part}} \lesssim 10^{11} h^{-1} M_{\odot}$ ), particularly at  $z \gtrsim 1$ . We observe

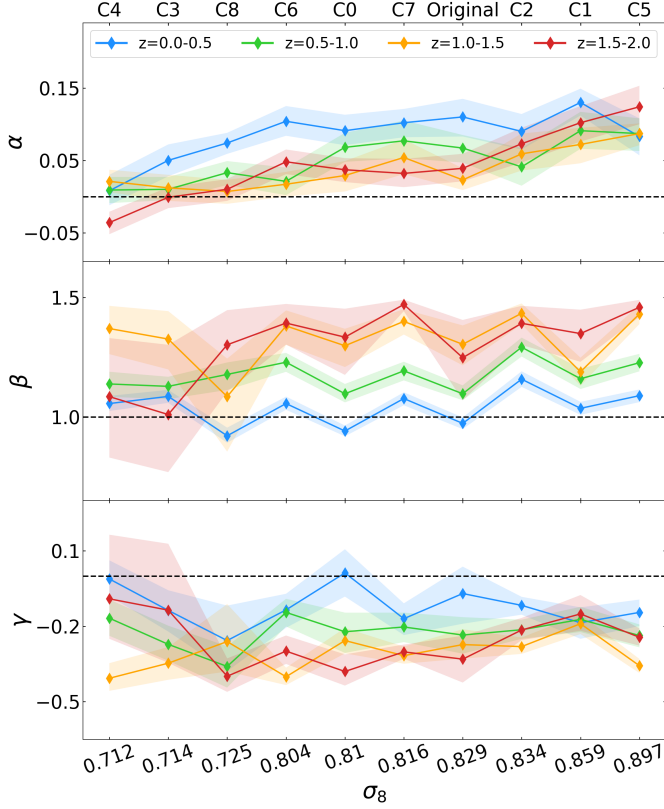


**Fig. 8.** Best-fit covariance-model parameters  $\alpha$  (top panel),  $\beta$  (middle panel), and  $\gamma$  (bottom panel) as a function of cosmology. Each color corresponds to a different redshift bin ( $z = 0.0-0.5, 0.5-1.0, 1.0-1.5, 1.5-2.0$ ) in the light cone, with shaded bands indicating the statistical uncertainties. The dashed black lines mark the reference values  $\alpha = 0, \beta = 1$ , and  $\gamma = 0$ . The cosmologies on the upper x-axis are sorted by increasing values of  $\sigma_8$ .

that insufficient mass resolution can bias the non-Poissonian shot-noise parameter by up to 30%.

- When started from the same initial random field, PINOCCHIO and OpenGADGET3 yield broadly consistent covariance estimates for the cluster 2PCF. Small discrepancies at the 5–10% level can be accounted for by modest shifts in the model’s nuisance parameters (see Eq.4). This demonstrates that PINOCCHIO can provide a reliable and computationally efficient alternative to full  $N$ -body simulations to measure clustering covariances for large cosmological surveys of galaxy clusters.
- Of the three calibrated nuisance parameters, only the non-Poissonian shot-noise correction  $\alpha$  shows a mild linear dependence on  $\sigma_8$ . The other parameters,  $\beta$  (bias rescaling) and  $\gamma$  (subleading shot-noise correction), exhibit more pronounced redshift and mass cut dependence than cosmology dependence.
- The redshift and mass cuts and redshift dependencies indicate that the survey selection function impacts the covariance calibration. Accurate modeling of the covariance for application to specific surveys thus requires realistic mocks replicating the observed selection to avoid systematic biases in cosmological inference.

Overall, our results confirm that this semi-analytical covariance model can robustly capture the main sources of uncertainty in cluster clustering, providing the nuisance parameters

are carefully tuned. In particular, approximate simulations such as PINOCCHIO can be employed effectively for such a calibration, enabling robust covariance estimates across diverse cosmological models and redshifts without incurring the computational expense of full  $N$ -body simulations.

## Data availability

The numerical data generated and analyzed in this study are not publicly available due to the large storage and computational resources required. The authors will make every reasonable effort to provide access to the underlying simulation outputs and derived data products upon request, subject to resource availability. The fiducial models for the HMF and halo bias used in this paper can be accessed in [Castro & Fumagalli \(2024\)](#).<sup>9</sup>

## Authors’ Contributions

The authors, A. Fumagalli and T. Castro, share co-authorship of this paper. T. Castro conceptualized and produced the simulated data, while A. Fumagalli carried out the formal analysis of the simulated data. All authors contributed to interpreting the results and writing the manuscript. All authors have read and approved the final version of the paper.

**Acknowledgements.** It is a pleasure to thank Isabella Baccarelli, Fabio Pitari, and Caterina Caravita for their support with the CINECA environment. This work is supported by the Agenzia Spaziale Italiana (ASI) under - Euclid-FASE D Attività scientifica per la missione - Accordo attuativo ASI-INAF n. 2018-23-HH.0, by the PRIN 2022 PNRR project “Space-based cosmology with Euclid: the role of High-Performance Computing” (code no. P202259YAF), by the Italian Research Center on High-Performance Computing Big Data and Quantum Computing (ICSC), a project funded by European Union - NextGenerationEU - and National Recovery and Resilience Plan (NRRP) - Mission 4 Component 2, by the INFN INDARK PD51 grant, and by the PRIN 2022 project EMC2 - Euclid Mission Cluster Cosmology: unlock the full cosmological utility of the Euclid photometric cluster catalog (code no. J53D23001620006). AF acknowledges support by the Excellence Cluster ORIGINS, which is funded by the Deutsche Forschungsgemeinschaft (DFG, German Research Foundation) under Germany’s Excellence Strategy - EXC-2094 - 390783311. AF acknowledges support from the Ludwig-Maximilians-Universität in Munich. The simulations were run partially on the Leonardo-Booster supercomputer as part of the Leonardo Early Access Program (LEAP) and under the ISCR initiative. We acknowledge the CINECA award for the availability of high-performance computing resources and support. We acknowledge the use of the HOTCAT computing infrastructure of the Astronomical Observatory of Trieste – National Institute for Astrophysics (INAF, Italy) (see [Bertocco et al. 2020](#); [Taffoni et al. 2020](#)).

## References

- Abell, P. A. et al. 2009 [arXiv:0912.0201]  
 Aghamousa, A. et al. 2016 [arXiv:1611.00036]  
 Allen, S. W., Evrard, A. E., & Mantz, A. B. 2011, ARA&A, 49, 409  
 Benson, B. A. et al. 2014, Proc. SPIE Int. Soc. Opt. Eng., 9153, 91531P  
 Berner, P., Refregier, A., Sgier, R., et al. 2022, JCAP, 11, 002  
 Bertocco, S., Goz, D., Tornatore, L., et al. 2020, in Astronomical Society of the Pacific Conference Series, Vol. 527, 303  
 Bocquet, S., Dietrich, J. P., Schrabback, T., et al. 2019, ApJ, 878, 55  
 Borgani, S., Rosati, P., Tozzi, P., et al. 2001, ApJ, 561, 13  
 Castro, T., Borgani, S., Dolag, K., et al. 2020, MNRAS, 500, 2316  
 Castro, T. & Fumagalli, A. 2024, CCToolkit: A Python Package for Cluster Cosmology Calculations  
 Chuang, C.-H. et al. 2015, MNRAS, 452, 686  
 Cohn, J. D. 2006, New Astron., 11, 226  
 Costanzi, M., Saro, A., Bocquet, S., et al. 2021, PRD, 103, 043522  
 Davis, M., Efstathiou, G., Frenk, C. S., & White, S. D. M. 1985, ApJ, 292, 371  
 Dolag, K., Borgani, S., Murante, G., & Springel, V. 2009, MNRAS, 399, 497  
 Euclid Collaboration: Castro, T., Fumagalli, A., Angulo, R. E., et al. 2023, A&A, 671, A100

<sup>9</sup> <https://github.com/TiagoBsCastro/CCToolkit>

- Euclid Collaboration: Castro, T., Fumagalli, A., Angulo, R. E., et al. 2024, *Astron. Astrophys.*, 691, A62
- Euclid Collaboration: Fumagalli, A., Saro, A., Borgani, S., et al. 2024, *A&A*, 683, A253
- Euclid Collaboration: Mellier, Y., Abdurro'uf, Acevedo Barroso, J. A., et al. 2024, *A&A*, in press (Euclid SI), arXiv:2405.13491
- Fumagalli, A., Biagetti, M., Saro, A., et al. 2022, *JCAP*, 12, 022
- Fumagalli, A., Costanzi, M., Saro, A., Castro, T., & Borgani, S. 2024, *A&A*, 682, A148
- Fumagalli, A., Saro, A., Borgani, S., et al. 2021, *A&A*, 652, A21
- Hitz, P., Berner, P., Crichton, D., Hennig, J., & Refregier, A. 2024 [arXiv:2410.01694]
- Hu, W. & Kravtsov, A. V. 2003, *ApJ*, 584, 702
- Kravtsov, A. & Borgani, S. 2012, *Ann. Rev. Astron. Astrophys.*, 50, 353
- Landy, S. D. & Szalay, A. S. 1993, *ApJ*, 412, 64
- Laureijs, R., Amiaux, J., Arduini, S., et al. 2011, arXiv:1110.3193
- Maartens, R., Abdalla, F. B., Jarvis, M., & Santos, M. G. 2015, *PoS, AASKA14*, 016
- Majumdar, S. & Mohr, J. J. 2004, *Astrophys. J.*, 613, 41
- Mana, A., Giannantonio, T., Weller, J., et al. 2013, *MNRAS*, 434, 684
- Marulli, F., Veropalumbo, A., & Moresco, M. 2016, *Astron. Comput.*, 14, 35
- Marulli, F. et al. 2018, *Astron. Astrophys.*, 620, A1
- Meiksin, A. & White, M. J. 1999, *MNRAS*, 308, 1179
- Michaux, M., Hahn, O., Rampf, C., & Angulo, R. E. 2021, *MNRAS*, 500, 663
- Monaco, P. 2016, *Galaxies*, 4, 53
- Monaco, P., Sefusatti, E., Borgani, S., et al. 2013, *MNRAS*, 433, 2389
- Monaco, P., Theuns, T., & Taffoni, G. 2002, *MNRAS*, 331, 587
- Munari, E., Monaco, P., Sefusatti, E., et al. 2017, *MNRAS*, 465, 4658
- Planck Collaboration XX: Ade, P. A. R., Aghanim, N., Armitage-Caplan, C., et al. 2014, *A&A*, 571, A20
- Planck Collaboration XXIV: Ade, P. A. R., Aghanim, N., Arnaud, M., et al. 2016, *A&A*, 594, A24
- Predehl, P. et al. 2021, *Astron. Astrophys.*, 647, A1
- Sartoris, B. et al. 2016, *MNRAS*, 459, 1764
- Schuecker, P., Bohringer, H., Collins, C. A., & Guzzo, L. 2003, *Astron. Astrophys.*, 398, 867
- Scoccimarro, R., Zaldarriaga, M., & Hui, L. 1999, *ApJ*, 527, 1
- Sellentin, E. & Starck, J.-L. 2019, *JCAP*, 08, 021
- Spergel, D. et al. 2015 [arXiv:1503.03757]
- Springel, V. 2005, *MNRAS*, 364, 1105
- Springel, V., Pakmor, R., Zier, O., & Reinecke, M. 2021, *MNRAS*, 506, 2871
- Springel, V., White, S. D. M., Tormen, G., & Kauffmann, G. 2001, *MNRAS*, 328, 726
- Taffoni, G., Becciani, U., Garilli, B., et al. 2020, in *Astronomical Society of the Pacific Conference Series*, Vol. 527, 307
- Takada, M. & Hu, W. 2013, *PRD*, 87, 123504
- To, C.-H. et al. 2021, *MNRAS*, 502, 4093
- Vikhlinin, A. et al. 2009, *Astrophys. J.*, 692, 1060
- Watson, W. A., Iliev, I. T., D'Aloisio, A., et al. 2013, *MNRAS*, 433, 1230